Chibuzo NNONYELU[1], Chinaza MADUKWE [2], Kosisochukwu MADUKWE [3]

Department of Electrical Engineering, University of Nigeria, Nsukka, Nigeria (1),
Department of Electrical and Electronic Engineering, Federal University of Agriculture, Makurdi, Benue, Nigeria (2),
School of Engineering and Computer Science Victoria University of Wellington, Wellington 6400, New Zealand (3)

Fully Steerable Collocated First-Order Cardioid Microphone Array Acoustic Beam-Pattern

Abstract. In the paper, a data-independent beamforming method capable of fully steering the mainlobe of the first-order cardioid triad is presented. This proposed method exploits the multi-pattern operating mode of the dual-diaphragm microphones design of some first-order cardioid microphones to extend the polar-azimuth space in to which the mainlobe of such cardioid triad to the full sphere. The beamwidth and directivity of the proposed collocated array are derived and analyzed.

Streszczenie. W artykule zaprezentowano metodę formowania wiązki akustycznej zdolnej do kierowania głównego listka triady w kształcie serca. Otrzymanie takiej charakterystyki umożliwia mikrofon z dwoma diafragmami. Analizowano szerokość i kierunkowość wiązki. (W pełni sterowalne formowanie wiązki akustycznej triady w kształcie serca)

Keywords: cardioid microphones, acoustic beam focusing, acoustic beam steering, acoustic signal processing, array signal processing, directional sensors,
Słowa kluczowe: mikrofon, wiązka akustyczna, charakterystyka w kształcie serca.

The Collocated Directional Sensor Array

Signal processing for arrays of spatially displaced sensors is usually frequency-dependent and can be complicated due to the ultra-wide band of acoustic signal. The frequency dependence of the array manifolds of such arrays emanates from the phase factor introduced by the spatial displacement of the constituent sensors, hence an array of spatially collocated sensors will eliminate the frequency dependence of the array manifold [1–3]. The concept of collocating directional sensors in orthogonal orientation has been proposed as the acoustic vector sensor/hydrophone in [3, 4]. The acoustic particle-velocity sensor has been implemented in Swallow float [5, 6], DIFAR (DIrectional Frequency Analysis and Recording) [7], and in other different forms in [8–12].

However, this method of eliminating the frequency dependence of the array manifold comes with a reduction in the aperture size of the array which translates to wide main lobes of its beam pattern. The use of microphones of relatively high directivity produces relatively narrower main lobes in the beam pattern of collocated microphone arrays. The first-order cardioid microphones are a family of highly directional microphones [13]. A collocated array of three first-order cardioid microphones whose constituent sensors are orthogonal was first proposed, and its spatial matched filter beam pattern studied by Wong et.al [1]. This beam pattern was shown to suffer from an inherent pointing bias and the inability of its mainlobe to be steered to all directions in the spherical coordinates. Another form of beamformer was proposed by Nnonyelu et. al [2] to eliminate the pointing bias but this array still suffers from an inability to be steered to all directions. This paper proposes a method that exploits the advantages of the dual-diaphragm microphones design or the differential microphone design of the first-order cardioid microphones to make the mainlobe of such first-order cardioid triad continuously steerable to any direction and with no pointing bias.

The Dual-Diaphragm Microphones

The first-order cardioid microphones can be realized in two ways: (a) as the weighted sum of the outputs of a pressure diaphragm (omnidirectional) and pressure-gradient diaphragm (figure-8) [13, see Chapter 5], (b) by acoustically delaying the wave incident from the rear of a single-diaphragm microphone; the front of the diaphragm is at $0°$ while the rear is at some angle between $0°$ and $180°$ [14]. The cardioid response pattern can also be realized by using

dual diaphragm approach as proposed and studied in [15]. Torio and Segota [15] showed that the dual-diaphragm design exhibits cardioid pattern at both higher and lower frequencies, almost independent of source proximity. Fig. 1 shows a sketch of the dual-diaphragm capsule. With the proper acoustic resistance and compliance, the desired first-order unidirectional shape can be achieved.
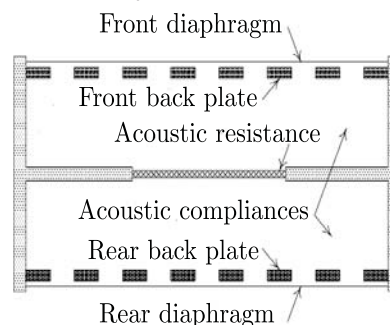

Fig. 1. A sketch of a dual-diaphragm capsule (Source: Torio and Segota 2000 [15]).

In multi-pattern operation mode, one diaphragm of the dual-diaphragm capsule can be used at a time, making it possible to have a cardioid polar pattern whose main axis can point in both front or rear direction. This polar gain pattern is mathematically represented as

$$(1) \qquad a \, = \, \alpha + \text{sign}(\xi)(1-\alpha)\cos\psi$$

where $\psi \in [0, 2\pi]$ is the angle between the direction of arrival and the axis of the sensor, and $\xi \in \mathcal{R}$ can be called the *diaphragm selector*. When $\xi > 0$, the front cardioid pattern is obtained; when $\xi < 0$, the rear cardioid pattern is obtained; and when $\xi = 0$, an omnidirectional pattern is obtained. Fig. 2 shows the plot of the gain pattern against the angle ψ for the hypercardioid and standard cardioid for both front and rear patterns.

The Cardioid Triad Array Manifold

Collocate and orient three of the dual-diaphragm cardioid microphones described in Section along the three axes of the Cartesian coordinates. The array manifold of such triad is given as

$$(2) \quad \mathbf{a}(\theta, \phi) \; = \; \begin{bmatrix} \alpha + \text{sign}(\xi)(1-\alpha)\cos(\phi)\sin(\theta) \\ \alpha + \text{sign}(\xi)(1-\alpha)\sin(\phi)\sin(\theta) \\ \alpha + \text{sign}(\xi)(1-\alpha)\cos(\theta) \end{bmatrix}$$
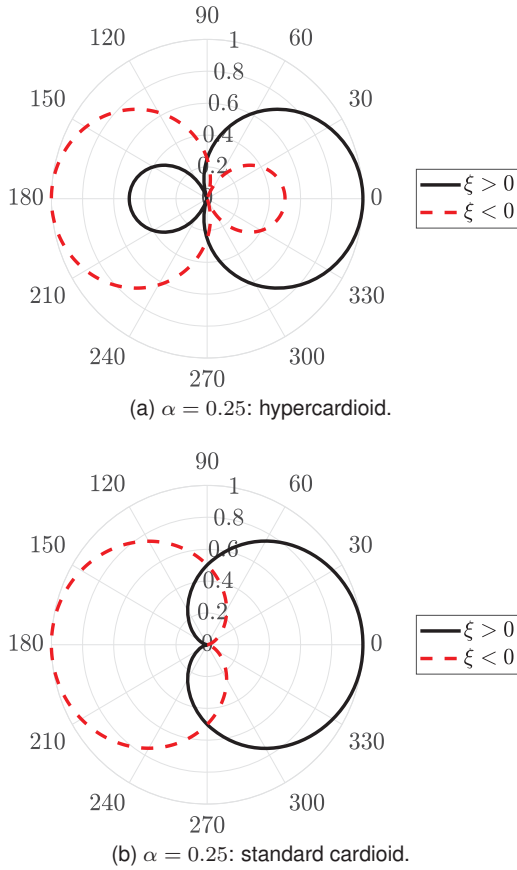
(a) $\alpha = 0.25$: hypercardioid.

(b) $\alpha = 0.25$: standard cardioid.

Fig. 2. Polar plots of a versus ψ for (a) hypercardioid, and (b) standard cardioid showing both front and rear polar patterns.

where the first, second, and third entries of the vector represent the gain patterns of the microphones in the x-, y-, and z- directions, respectively; $\theta \in [0, \pi]$ is the polar angle measured from the positive z-axis and $\phi \in [0, 2\pi]$ is the azimuth angle measured from the positive x-axis. The above vector (2) does not contain a frequency term, as expected of the collocated sensor array. The collocation decoupled the frequency and direction of arrival information of the array's output. This has been proposed and studied for single-diaphragm cardioid microphones (i.e $\xi > 0$) in [1, 2]. By defining the direction cosines $u := \cos(\phi)\sin(\theta), v := \sin(\phi)\sin(\theta)$, and $w := \cos(\theta)$, the array manifold (2) is alternatively expressed as

$$(3) \qquad \mathbf{a}(u,v,w) = \begin{bmatrix} \alpha + \text{sign}(\xi)(1-\alpha)u \\ \alpha + \text{sign}(\xi)(1-\alpha)v \\ \alpha + \text{sign}(\xi)(1-\alpha)w \end{bmatrix}$$

The Array's Beam-Pattern

A simple data-independent beamformer was proposed and analyzed for a cardioid triad as [2]

$$(4) \quad \mathbf{w} = \begin{bmatrix} u_{\text{look}} \\ v_{\text{look}} \\ w_{\text{look}} \end{bmatrix} := \begin{bmatrix} \cos(\phi_{\text{look}})\sin(\theta_{\text{look}}) \\ \sin(\phi_{\text{look}})\sin(\theta_{\text{look}}) \\ \cos(\theta_{\text{look}}) \end{bmatrix}$$

where $\theta_{\text{look}} \in [0, \pi]$ and $\phi_{\text{look}} \in [0, 2\pi]$ are the look-direction's polar angle and azimuth angles respectively. The output of this beamformer

$$\begin{aligned} B &= \mathbf{w}^T \mathbf{a}(u,v,w) \\ &= \alpha g_{\text{look}} + \text{sign}(\xi)(1-\alpha)\left(u_{\text{look}}u + v_{\text{look}}v \right. \\ (5) & \qquad \left. + w_{\text{look}}w\right) \end{aligned}$$

where $g_{\text{look}} := u_{\text{look}} + v_{\text{look}} + w_{\text{look}}$.

The beamformer's output is a dot product of two vectors, hence its maximum value occurs at $(u_{\max}, v_{\max}, w_{\max}) = (u_{\text{look}}, v_{\text{look}}, w_{\text{look}})$ and minimum value $(u_{\min}, v_{\min}, w_{\min}) = (-u_{\text{look}}, -v_{\text{look}}, -w_{\text{look}})$.

For the triad of single-diaphragm cardioid proposed in [2], the location of the mainlobe would point diametrically opposite the look direction for $g_{\text{look}} < 0$ (i.e look directions whose sum of direction cosine is less than zero), in its absolute magnitude pattern $|B|$. This problem is due to the inability of the constituent single-diaphragm cardioid microphones to produce a rear cardioid pattern. The problem is solved by the use of dual-diaphragm microphones.

The use of dual-diaphragm microphones operated in multi-pattern mode requires a control signal to switch between the front or rear diaphragms when needed. Since the pointing bias for the triad of single-diaphragm cardioid microphones occurs when $g_{\text{look}} < 0$ (beamformer's parameter), and $\xi < 0$ (microphone parameter) selects the rear diaphragm for the microphones, equating the two automates the switching thereby eliminating the pointing bias as mathematically show subsequently.

By equating the diaphragm selector ξ to g_{look},

$$\begin{aligned} B &= \alpha g_{\text{look}} + \text{sign}(g_{\text{look}})(1-\alpha)\left(u_{\text{look}}u + v_{\text{look}}v \right. \\ & \qquad \left. + w_{\text{look}}w\right) \\ &= \text{sign}(g_{\text{look}})\left(\alpha|g_{\text{look}}| + (1-\alpha)\left(u_{\text{look}}u + \right.\right. \\ (6) & \qquad \left.\left. v_{\text{look}}v + w_{\text{look}}w\right)\right) \end{aligned}$$

The magnitude beampattern $|B|$ studied in [2] was shown to not always have a peak in all look directions (see Section II.B of [2]). In this proposed array, there always exists a peak in the magnitude pattern $|B|$ for all look direction and α as

$$\begin{aligned} B_{(u,v,w)=(u_{\text{look}}, v_{\text{look}}, w_{\text{look}})} &> 0 \\ \implies \alpha|g_{\text{look}}| + (1-\alpha) &> 0 \\ (7) \qquad \implies |g_{\text{look}}| &> \frac{-(1-\alpha)}{\alpha} \end{aligned}$$

which is true $\forall g_{\text{look}}$ and $\forall \alpha$ as the left hand side of (7) is always positive and greater than its right hand side which is always negative. Therefore, the beampattern of the orthogonal triad of dual-diaphragm cardioid microphones suffers no pointing bias.

Half-Power Beam Width

The beampattern of the cardioid triad has been shown to be rotationally symmetric about an axis from origin through its mainlobe [1, 2]. The half-power beamwidth is also defined here as the surface area of the spherical cap whose base is the contour made by the half-power points on the beampattern. For some values of α, all points on the beam pattern are above the half-power value ($|B_{\max}|/\sqrt{2}$). Hence the half-power beamwidth is defined for only the values of α and g_{look} such that all points on the beam pattern are not above the half-power value, i.e.

$$\begin{aligned} B_{\min} &\leq B_{\max}/\sqrt{2} \\ (8) \qquad \implies |g_{\text{look}}| &\leq \frac{\sqrt{2}+1}{\sqrt{2}-1}\frac{(1-\alpha)}{\alpha}. \end{aligned}$$

The condition (8) will always hold $\forall g_{\text{look}}$ for only $\alpha \leq \frac{\sqrt{2}+1}{\sqrt{3}(\sqrt{2}-1)+(\sqrt{2}+1)} \approx 0.7709$. Therefore, all the commercially available cardioids $\alpha = 0.25$ –hypercardioid,
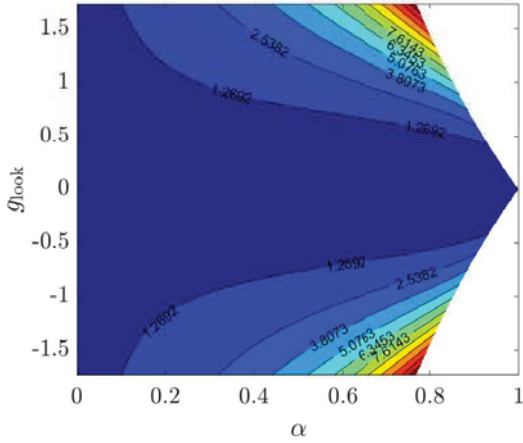
Fig. 3. Plot of the beamwidth versus α and g_{look}. The blank areas depict regions where all the points on the beampattern are greater than $B_{\max}/\sqrt{2}$.

$\alpha \approx 0.37$ – supercardioid, $\alpha = 0.5$ –standard cardioid, and $\alpha = 0.7$ – subcardioid are covered.

Given a sphere of radius $|B_{\max}|/\sqrt{2}$, the half-power beamwidth is the surface area of the spherical cap whose base is the closed contour formed by the intersection of the sphere and the points on the beampattern's mainlobe equal to $B_{\max}/\sqrt{2}$. Thus, the beamwidth

$$(9) \quad \mathrm{BW} = \pi \frac{\sqrt{2} - 1}{\sqrt{2}(1 - \alpha)} \left(\alpha|g_{\mathrm{look}}| + (1 - \alpha)\right)^3.$$

Plot of the beamwidth BW versus α and g_{look} is shown in Fig. 3. The blank areas depict regions where all the points on the beampattern are greater than $B_{\max}/\sqrt{2}$, i.e. the regions in the $(\alpha, g_{\mathrm{look}})$-space that violate the condition given in (8). For any α, the beamwidth is minimum when $g_{\mathrm{look}} = 0$ and maximum when $|g_{\mathrm{look}}| = \sqrt{3}$. The $|g_{\mathrm{look}}| = \sqrt{3}$ translates to $(u_{\mathrm{look}}, v_{\mathrm{look}}, w_{\mathrm{look}}) = \pm \left(\frac{1}{\sqrt{3}}, \frac{1}{\sqrt{3}}, \frac{1}{\sqrt{3}}\right)$, which is equivalent to $(\theta_{\mathrm{look}}, \phi_{\mathrm{look}}) = (54.74°, 45°)$ and $(\theta_{\mathrm{look}}, \phi_{\mathrm{look}}) = (125.26°, 225°)$ (see Fig. 4).
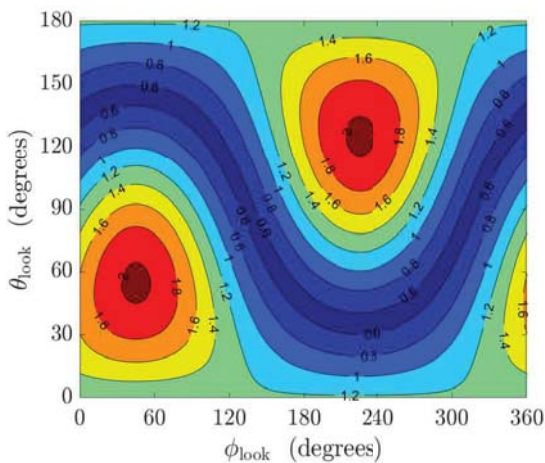
Fig. 4. Plot of the beamwidth versus look-direction polar angle θ_{look} and look-direction azimuth angle ϕ_{look} for $\alpha = 0.25$.

Directivity

The directivity of a sensor-array is the array's directive gain, in an isotropic noise field, when the array is steered towards a look direction $(\theta_{\mathrm{look}}, \phi_{\mathrm{look}})$. The directivity of an array is beamformer-dependent, and according to [16], direc-
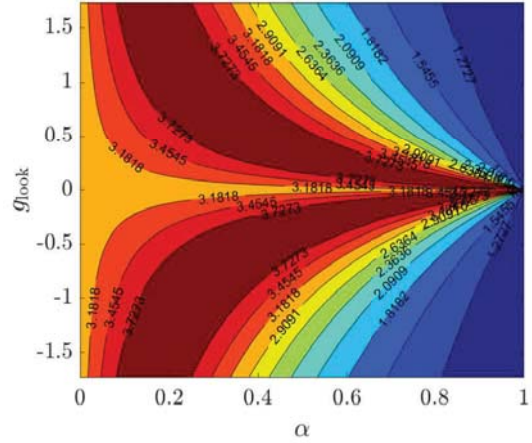

Fig. 5. Plot of the directivity versus α and g_{look}.

tivity is defined as

$$(10) \quad D = \frac{4\pi B^2_{(\theta,\phi)=(\theta_{\mathrm{look}},\phi_{\mathrm{look}})}}{\int_0^\pi \int_0^{2\pi} \sin(\theta) B^2 \, d\theta \, d\phi}.$$

Substituting the beamformer output B from (6) and evaluating the integral (10)

$$(11) \quad D = \frac{3(\alpha|g_{\mathrm{look}}| + (1 - \alpha))^2}{(1 - \alpha)^2 + 3\alpha^2|g_{\mathrm{look}}|^2}$$

Plot of the directivity versus α and g_{look} is shown in Fig. 5 and also plotted versus look direction's polar angle θ_{look} and azimuth angle ϕ_{look} for different values of α in Fig. 6. The directivity of this array is symmetric about $g_{\mathrm{look}} = 0$, which determines the switching between front and rear diaphragm (see Fig. 5). There is increase in variation with g_{look}, (i.e. look direction) as the dynamic range of the directivity increases with α (see Fig. 6c - Fig. 6d).

To determine the direction that gives the maximum and minimum directivity, the first derivative is used to obtain the critical points, and second derivative test used to establish the natures of the critical points. Hence, the maximum directivity occurs at

$$(12) \quad |g_{\mathrm{look}}| = \frac{(1 - \alpha)}{3\alpha},$$

with the value of 4. The minimum directivity occurs at

$$(13) \quad |g_{\mathrm{look}}| = \begin{cases} 0 & \text{if } \alpha \in (0, \frac{1}{2}(\sqrt{3} - 1)] \\ \sqrt{3} & \text{if } \alpha \in (\frac{1}{2}(\sqrt{3} - 1), 1) \end{cases},$$

with minimum values of $D = 3$ for $\alpha \in (0, \frac{1}{2}(\sqrt{3} - 1)]$, and $D = 1 + \frac{2(1-\alpha)^2 + 6\sqrt{3}\alpha(1-\alpha)}{9\alpha^2 + (1-\alpha)^2}$ for $\alpha \in (\frac{1}{2}(\sqrt{3} - 1), 1)$. Therefore, the least directivity which occurs when $\alpha = 1$ is equal to one which implies that the directivity never gets to zero. This is because the microphone is switched to the other diaphragm before getting to zero directivity. This feature is not present in the directivity of the array discussed in [2].

The directivity of the tri-axial velocity sensor (also known as acoustic vector sensor) is 3, and is constant over the polar and azimuth angle space. This can be obtained by setting $\alpha = 0$ in (11). The cardioid triad proposed in this paper attains directivity as high as 4 is some look direction for $\alpha \in (0, 1)$ i.e. excluding the figure-8 $\alpha = 0$ and omnidirectional array $\alpha = 1$, with some having directivity of 3 as the least directivity. That is, $D \geq 3$ if and only if $|g_{\mathrm{look}}| \leq \frac{1-\alpha}{\alpha}$, a
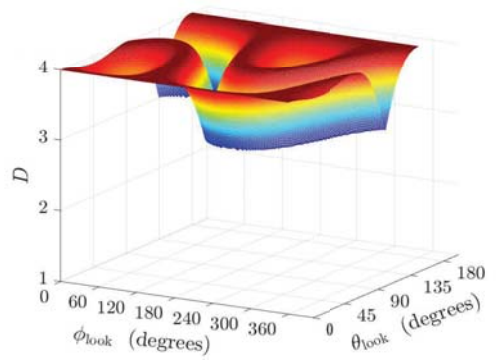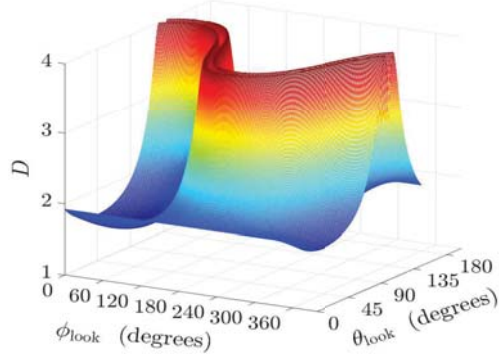
(a) $\alpha = 0.25$: hypercardioid.
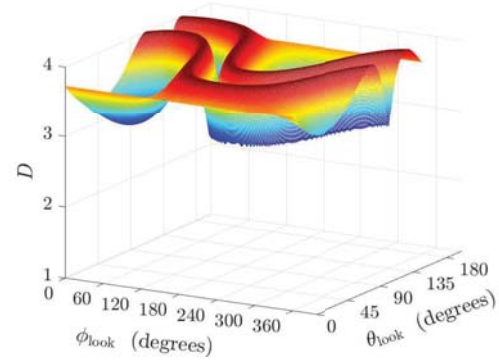
(b) $\alpha = \frac{1}{2}(\sqrt{3} - 1)$: supercardioid.
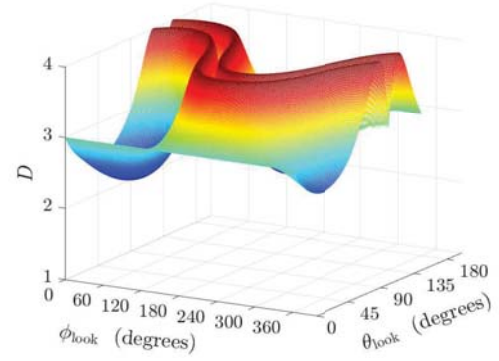
(c) $\alpha = 0.5$: standard cardioid.

(d) $\alpha = 0.7$: sub cardioid.

Fig. 6. Plots of directivity D versus look direction's polar angle θ_{look} and azimuth angle ϕ_{look} for (a) $\alpha = 0.25$: hypercardioid, (b) $\alpha = \frac{1}{2}(\sqrt{3} - 1)$: super cardioid, (c) $\alpha = 0.5$: standard cardioid and (d) $\alpha = 0.7$: sub cardioid.

condition that is always true for only $\alpha \in (0, (\sqrt{3} - 1)/2]$ which includes the hypercarioid and supercardioid microphones. The hypercardioid and supercardioid always outperform the figure-8 array in all look directions in terms of directivity. This is because they are less sensitive at their sides and directly behind them, unlike the figure-8 that is equally sensitive to sounds arriving from both front and rear, and also is more sensitive on its sides compared to the hypercardioid and supercardioid. The hypercardioid ($\alpha = 0.25$) has more of its directivity close to 4 as can be seen in Fig. 6a, and Fig. 5 where a line along $\alpha = 0.25$ cuts more red part of the contour than other values of α. With more of its directivity close to 4, the hypercardioid triad is the best choice for speech pickup in sound reinforcement systems as it provides the highest rejection, relative to the look direction, of randomly arriving reverberant sounds.

Conclusion

A data-independent beamformer has been proposed for a collocated and orthogonal first-order cardioid microphone triad which exploits a feature of the dual-diaphragm cardioid microphone to eliminate the problem of limited polar-azimuth space of the mainlobe of the spatial-matched-filter beamformer. The control signal for switching between the diaphragms of the constituent microphones is equated to the sum of the direction cosines of the look direction of the beamformer making it possible to achieve the front-back symmetry in the proporties of the beam pattern. The beamwidth and directivity of the array were derived and studied. The cardioid array has higher directivity compared to the figure-8 tri-axial sensor such as the acoustic velocity sensor, while exhibiting higher beamwidth in some look direction of the beamformer.

Authors: Dr. Chibuzo Nnonyelu, Department of Electrical Engineering, University of Nigeria, Nsukka, 410001 Enugu, Nigeria. email: chibuzo.nnonyelu@unn.edu.ng
Chinaza Madukwe, Department of Electrical and Electronic Engineering, Federal University of Agriculture, Markurdi, Benue, Nigeria. email: Madukweca@gmail.com
Kosisochukwu Madukwe, School of Engineering and Computer Science Victoria University of Wellington, PO Box 600, Wellington 6400, New Zealand email: Kosisochukwu.madukwe@ecs.vuw.ac.nz

REFERENCES

[1] Wong K. T. , Nnonyelu C. J. , and Wu Y. I.: A triad of cardioid sensors in orthogonal orientation and spatial collocation – its spatial-matched-filter-type beam-pattern, IEEE Transactions on Signal Processing, 66(4), pp. 895–906, February 2018.
[2] Nnonyelu C. J., Wong K. T., and Wu Y. I.: Cardioid microphones/hydrophones in a collocated/orthogonal triad – a new beamformer with no beam-pointing error, The Journal of the Acoustical Society of America, 145(1), pp. 575–588, January 2019.
[3] Nehorai A. and Paldi E. : Acoustic vector-sensor array processing, IEEE Transactions on Signal Processing, 42(9), pp. 2481–2491, September 1994.
[4] Wong K. T. and Zoltowski M. D.: Closed-form underwater acoustic direction-finding with arbitrarily spaced vector hydrophones at unknown locations, IEEE Journal of Oceanic Engineering, 22(4), pp. 649–658, October 1997.
[5] D'Spain G. L. , Hodgkiss W. S. , and Edmonds G. L. : Energetics of the deep ocean's infrasonic sound field, The Journal of the Acoustical Society of America, 89(3), pp. 1134–1158, March 1991.
[6] D'Spain G. L., Hodgkiss W. S., and Edmonds G. L.: The simultaneous measurement of infrasonic acoustic particle velocity and acoustic pressure in the ocean by freely drifting Swallow floats, IEEE Journal of Oceanic Engineering, 16(2), pp. 195–207, April 1991.

[7] Nickles J. C. , Edmonds G., Harriss R., Fisher F., Hodgkiss W. S., Giles J., and D'Spain G.: A vertical array of directional acoustic sensors, in OCEANS 92 Proceedings: Mastering the Oceans Through Technology, 1, August 1992, pp. 340–345.

[8] Mathew V., Idichandy V. G., and Bhattacharyya S. K.: A perforated-ball velocity meter for underwater kinematics measurement in waves and current, in Proceedings of the 2000 International Symposium on Underwater Technology (Cat. No.00EX418), pp. 218–223, May 2000.

[9] Nnonyelu C. J. and Morris Z. N.: Acoustical direction finding using a bayesian regularized multilayer perceptron artificial neural networks on a tri-axial velocity sensor, International Journal of Mechatronics, Electrical and Computer Technology, 10(35), January 2020.

[10] McEachern J. F., McConnell J. A., Jamieson J., and Trivett D.: Arap - deep ocean vector sensor research array, in OCEANS 2006, pp. 1–5, 2006, .

[11] Shipps J. C. and Deng K.: A miniature vector sensor for line array applications," in Oceans 2003. Celebrating the Past ... Teaming Toward the Future (IEEE Cat. No.03CH37492), 5, pp. 2367–2370, 2003.

[12] Yntema D. R., Druyvesteyn W. F., and Elwenspoek M.: A four particle velocity sensor device, The Journal of the Acoustical Society of America, 119(2), pp. 943–951, February 2006.

[13] Eargle J., *The Microphone Book*, 2nd ed. Massachusetts: Focal Press, 2005.

[14] Ballou G., Ciaudelli J., and Schmitt V., *Electroacoustic Devices: Microphones and Loudspeakers*, G. Ballou, Ed. Oxford, UK: Focal Press, 2009.

[15] Torio G. and Segota J.: Unique directional properties of dual-diaphragm microphones, Engineering, 2000.

[16] Huang Y. and Benesty J., Eds., *Audio Signal Processing for Next-Generation Multimedia Communication Systems*. Boston: Kluwer Academic Publishers, 2004.